Phase-space resolved measurements of the influence of RF heating and MHD instabilities on the fast-ion distribution in ASDEX Upgrade

M. Weiland[1], B. Geiger[1], R. Bilato[1], G. Tardini[1], A. Jacobsen[2], S. K. Nielsen[2], F. Ryter[1], M. Salewski[2], H. Zohm[1], the ASDEX Upgrade team[1] and the EUROfusion MST1 team*

[1]Max-Planck-Institut für Plasmaphsyik, Garching, Germany
[2]Technical University of Denmark, Lyngby, Denmark

Corresponding Author: markus.weiland@ipp.mpg.de

Abstract:

Recent improvements of the FIDA (Fast-Ion D-Alpha) diagnostic in ASDEX-Upgrade make possible the tomographic reconstruction of the distribution function of fast ions at several radial positions on the low-field side. Here, the results of two applications of this upgraded FIDA diagnostic are presented. The first application is to study the evolution of the fast-ion distribution function during sawtooth crashes. It clearly shows that ions with high energies and pitch values ($v_\parallel/v$) close to zero are less affected by the sawtooth activity. This feature can be explained by the fact that these ions are weakly bound to the (reconnecting) magnetic field lines. As second application, we investigate the acceleration of fast deuterium ions by 2^{nd} harmonic ion cyclotron resonance heating. In this ICRH scenario, hydrogen is resonant at the first harmonic, which is in competition with deuterium absorption and needs to be considered in the data analysis. Here, the FIDA tomography can be interpreted as sum of the D and H distribution function, if it is written as function of E/m. In an NBI+ICRH phase, the tomographic reconstructions in the plasma center yield two distinct high-energy tails above the NBI energy, which are not present in a NBI-only phase.

1 Introduction

Fast ions are generated in present-day tokamaks by neutral beam injection and ion cyclotron resonance heating, and are used for plasma heating and current drive. In future fusion devices, energetic α-particles from fusion reactions will be the main heating mechanism. Hence, it is crucial to understand the transport behavior and creation mechanisms of fast ions.

A way to measure the fast-ion distribution is the FIDA (fast-ion D-alpha) diagnostic, which analyzes the Doppler-shifted D-alpha radiation of neutralized fast-ions spectroscopically. With lines of sight at different radial positions, radial fast-ion density profiles can be measured. At the same time, the shape of the Doppler spectrum contains information about the 2D velocity space distribution $f(E, v_\parallel/v)$. Observation from different viewing angles allows consequently a tomographic reconstruction of $f(E, v_\parallel/v)$ at each radial position (defined by the line of sight geometry). Thus, the FIDA tomography has the unique feature that the fast-ion phase-space can be observed with simultaneous real-space and

*See appendix of H. Meyer et.al. (OV/P-12) Proc. 26th IAEA Fusion Energy Conf. 2016, Kyoto, Japan

velocity-space resolution. To facilitate this, the FIDA diagnostic at ASDEX Upgrade has been upgraded from two to five views since the 2014 experimental campaign, and the spectrometer has been upgraded to measure blue and red Doppler shifts simultaneously. These novel diagnostic capabilities are used to study the effect of sawtooth crashes on the fast-ion velocity distribution and the further acceleration of fast D ions by 2nd harmonic ion cyclotron heating.

2 Diagnostic setup

The FIDA diagnostic at ASDEX Upgrade [1, 2, 3] consists now of five viewing arrays (see fig. 1). Each view has several radially distributed lines of sight (LOS), and has a different angle towards the magnetic field Φ. The latter determines the observed region in velocity space, and hence an equal distribution of angles (in the plasma center) has been chosen: $\Phi \approx 10°, -20°, -50°, 70°$ and $85°$. The FIDA spectrometers are capable of measuring the blue- and red-shifted part of the D-alpha spectrum simultaneously, and have a capacity of up to 37 viewing channels. Each wavelength λ in the FIDA spectrum can be interpreted as a weighted integral of the fast-ion velocity distribution $f(E, \xi)$:

$$FIDA(\lambda) = \int_0^\infty \int_{-1}^{+1} W(\lambda, E, \xi) f(E, \xi)\, \mathrm{d}E \mathrm{d}\xi \quad (1)$$

Hereby, the pitch is denoted with $\xi = v_\parallel / v$. The so called weight functions W can be calculated with the FIDASIM code [4, 5]. In fig. 2, weight functions are shown for five FIDA views in the plasma center and two wavelengths corresponding to Doppler-shifts $\Delta\lambda = \pm 3.9$ nm. Weight functions at different Doppler-shifts have typically similar shapes, but are shifted with respect to the energy. It can be seen that the velocity space is well covered. This allows a tomographic reconstruction of $f(E, \xi)$. Therefore, eq. 1 is discretized to a matrix equation $\vec{s} = W\vec{f}$. The tomography can then be calculated from the FIDA signals $\vec{s}$ by $\vec{f} = W^+\vec{s}$, where W^+ is calculated by first order Tikhonov regularization [6]. This is equivalent to calculating a least-squares fit with the additional condition that the solution f should have small gradients. In addition, negative values are damped by an iterative method (described in [2, 3]).

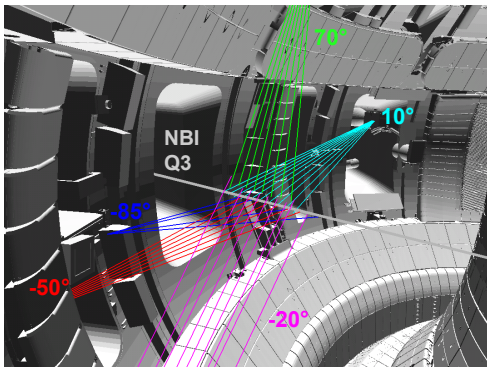

FIG. 1: 3D visualization of the five FIDA line of sight arrays.

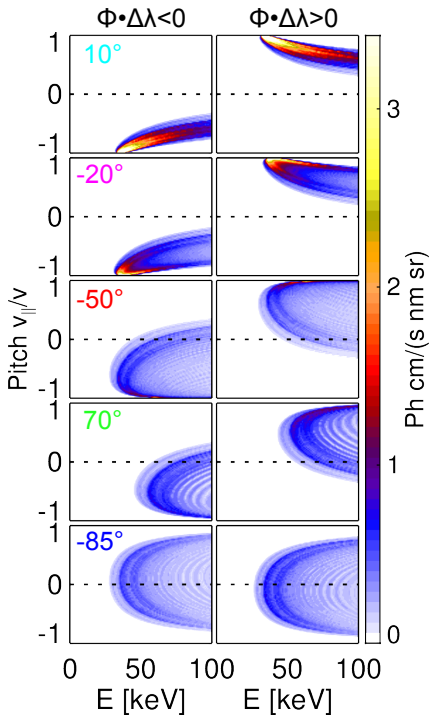

FIG. 2: Weight functions of the five FIDA views and two Doppler-shifts $\Delta\lambda = \pm 3.9$ nm.

3 Fast-ion redistribution by sawtooth crashes

Sawtooth crashes can strongly redistribute fast ions, which has been demonstrated e.g. from FIDA [7] or neutron measurements [8]. However, theoretic models [9, 10, 11] predict that the redistribution strength depends on the fast-ion velocity. In particular, fast ions with high drift velocities are expected to be more weakly redistributed. With the improved FIDA setup and the additional views, it is now possible to investigate the velocity dependence of this redistribution experimentally.

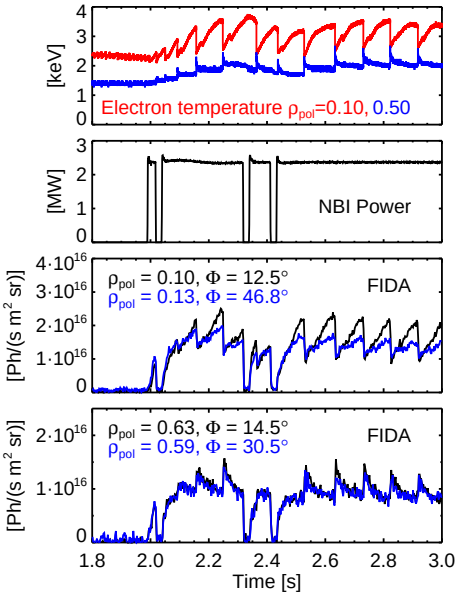

FIG. 3: Representative timetraces of ASDEX Upgrade discharge #31557. The FIDA raw signals are obtained by integrating the spectra over Doppler-shifts $\Delta\lambda = [3.7, 5.0]$ nm

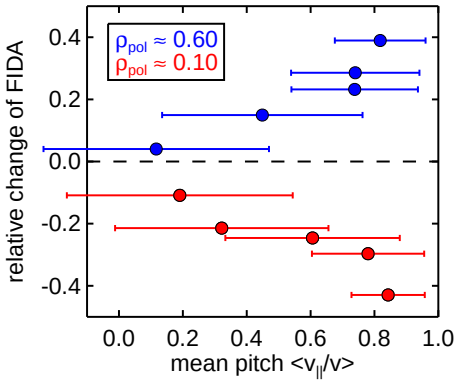

FIG. 4: Relative change of the FIDA emission ($|\Delta\lambda| = [3.5, 4.5]$ nm) *during the sawtooth crash at 2.25s. The x-axis refers to the average pitch observed by the line of sight. It is calculated by integrating the weight functions over the relevant energies (20-60 keV) and wavelength range:* $g(\xi) = \int_{\lambda_1}^{\lambda_2}\int_{E_1}^{E_2} W(\lambda, E, \xi)\, d\lambda dE$. *The mean value of* $g(\xi)$ *is plotted as dot, and the standard deviation is shown with error bars.*

We have analyzed discharge #31557. The discharge was run with a magnetic field of -2.6 T and a plasma current of 1 MA. Fig. 3 shows time traces of the central and mid-radius electron temperature, where strong sawtooth activity can be identified. The mid-radius time trace shows an temperature increase with each sawtooth crash, and hence lies outside of the inversion radius. The time trace of the NBI (Q3) and the FIDA raw signals for central and mid-radius LOS are shown below. The onset of NBI is followed by a rise of the FIDA radiation, which can be identified with the fast-ion density build-up. Later on, the FIDA radiation drops in the plasma center with each sawtooth crash, and rises in the outer lines of sight. This indicates a strong redistribution of the fast ions due to the crash. From the raw signals, it is already observable that the central $\Phi \approx 10°$ LOS, which sees mostly co-current fast ions, measures the strongest sawtooth drop, while the FIDA views, which observe more strongly gyrating fast ions have smaller sawtooth drops.

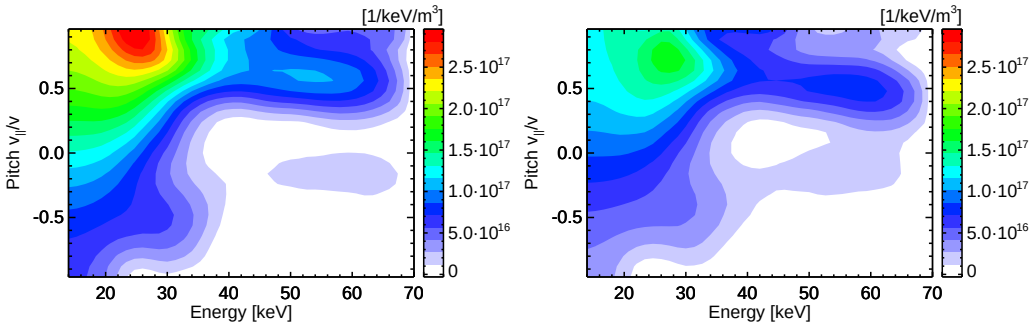

(a) Plasma center $\rho_{\mathrm{pol}} \approx 0.10$

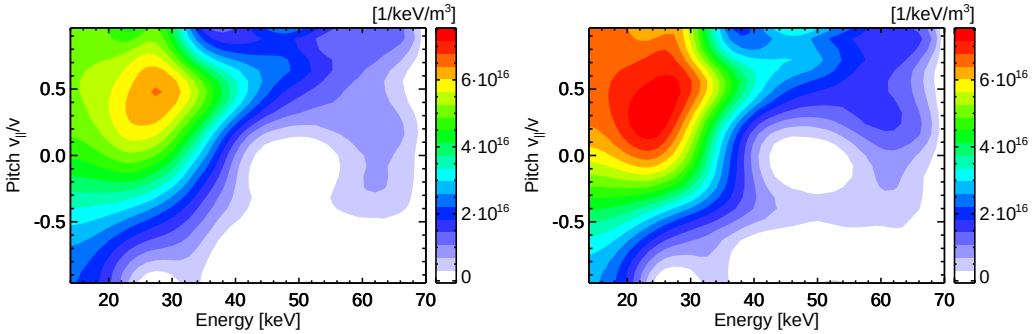

(b) $\rho_{\mathrm{pol}} \approx 0.60$

FIG. 5: Tomographic reconstruction of $F(E, v_{\parallel}/v)$ from FIDA measurements before (left) and after the sawtooth crash at 2.25s in #31557.

Outside of the inversion, the $\Phi \approx 10°$ projection shows a stronger rise of FIDA radiation than a $\Phi \approx 30°$ projection.

This can be seen more clearly in figure 4, where the relative change ((after-before) / before) of the FIDA emission during the sawtooth crash at 2.25s is shown for five FIDA views and for the two radial positions as a function of the mean observed pitch. These observations give the indication, that fast ions with high pitches $v_{\parallel}/v$ are more strongly expelled from the plasma center than fast ions with low pitches. This can be studied more quantitatively with the FIDA tomography method.

We have performed tomographic reconstructions before and after the sawtooth at 2.25s from five FIDA views, which measure all approximately at the same radial position. The calculation was carried out for a set of LOS in the plasma center ($\rho_{\mathrm{pol}} \approx 0.10$) and a second set of five views outside of the sawtooth inversion ($\rho_{\mathrm{pol}} \approx 0.60$). Regions with impurity lines and beam emission are excluded for the tomography, as well as the wavelength range [-3.1 nm, +3.1nm] around the D-alpha line, which is dominated by thermal ions.

The results of the tomography are shown in fig. 5. From the reconstruction, it is possible to determine the total fast-ion density (of fast ions above 24 keV), and thus quantify the effect of the sawtooth: In the plasma center, it causes a 25% drop of total fast-ion density, while at $\rho_{\mathrm{pol}} = 0.60$ an increase of 19% is observed. With a cut of the fast-ion distribution function at constant energy, we can estimate how this total density

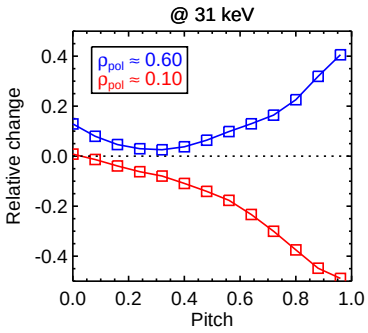

FIG. 6: Pitch distribution of the relative change of $F(E = 31\ \mathrm{keV}, v_\parallel/v)$.

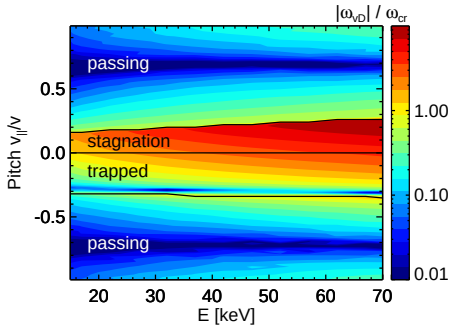

FIG. 7: Ratio of helical precession $|\omega_{vD}|$ and angular crash frequency ω_{cr}.

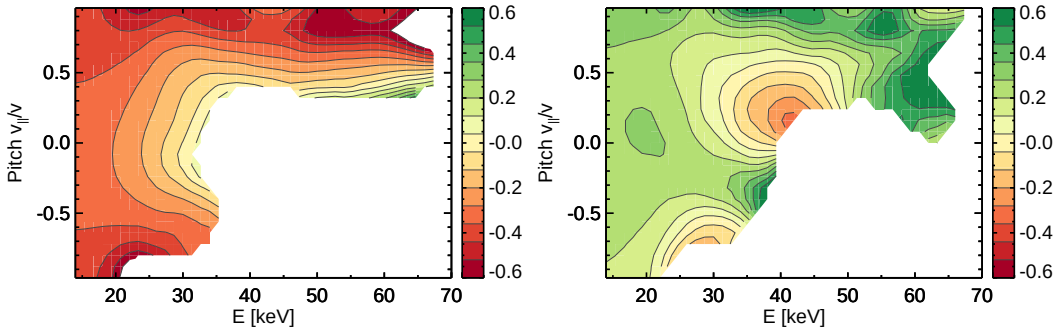

(a) $\rho_{\mathrm{pol}} = 0.10$ **(b)** $\rho_{\mathrm{pol}} = 0.60$

FIG. 8: Relative change $(F_{after} - F_{before})/F_{before}$ at two different radial positions in and outside of the sawtooth inversion (corresponding to fig. 5). The relative difference is only well defined, if $F_{before}(E, \xi)$ is high enough. Therefore, only regions which fulfill $F_{before}(E, \xi) \geq 0.15 \cdot \max(F_{before})$ are shown.

changes are distributed along different pitches (fig. 6). It can be seen that fast ions with high pitches are much stronger expelled from the plasma core (-50%), while more strongly gyrating fast ions with pitches close to 0 are much less affected by the sawtooth. This is in accordance with [12], where a FIDA tomography is calculated with singular value decomposition from four FIDA views in the plasma center, and a similar pitch distribution of the density change is found.

Outside of the sawtooth inversion at $\rho_{\mathrm{pol}} = 0.60$, a strong increase is found for fast ions with high pitches (+40%), while at the same time, only little changes are observed for strongly gyrating fast ions with pitches close to 0.

We can get a more detailed picture of the redistribution by calculating the relative change for the entire velocity space. This is shown for both radial positions in figure 8. The relative difference is only well defined, if $F_{\mathrm{before}}(E, \xi)$ is high enough. Therefore we have calculated it only for regions which fulfill $F_{\mathrm{before}}(E, \xi) \geq 0.15 \cdot \max(F_{\mathrm{before}})$. It can be seen that the absolute value of the relative change is largest for pitches close to +1 for all energies, and weaker for fast ions with pitches around 0. It is hard to make a

robust statement for fast ions with very negative pitches, because there are very few fast ions due to to co-current orientation of the neutral beams. At least in the plasma center, it seems that the strength of fast-ion redistribution is more or less symmetrical with respect to $\xi = 0$. For low energies, the pitch dependence of the sawtooth redistribution is rather weak, as it is expected for thermal particles. This pitch dependence seems to increase with energy - and a region around $\xi = 0$ with very weak redistribution is seen towards higher energies. Outside of the inversion radius an overall similar shape of the relative change is found with opposite sign. This can be interpreted such that the ions from the core are redistributed further outside, keeping their energy and magnetic moment more or less constant. There are some small scale structures visible close to the $F_{\mathrm{before}}(E, \xi) \geq 0.15 \cdot \max(F_{\mathrm{before}})$ boundary, which should be treated with care, since the region close to that boundary has larger uncertainties and the outer measurement position has less fast ions in general. The rather broad region with high redistribution around $E = 60$ keV$, \xi = 0.5$ might be explainable by the fact that the full energy component (60 keV) of the beam is more strongly deposited in the plasma center. Hence, redistribution of those particles towards the mid-radius causes a stronger relative increase there.

The observed pitch-angle dependence can be explained by theoretical considerations [9, 10, 11] by the fact that ions with low $\left|v_\parallel / v\right|$ have large drift velocities (compared to their parallel velocity) and are thus more weakly bound to the (reconnecting) magnetic field lines. More precisely, the ratio of the timescales of the drift motion and the sawtooth crash duration (estimated from soft-X-ray data: $\tau_{\mathrm{cr}} \approx 80$ µs) is relevant. Fig. 7 shows a ratio of the corresponding angular frequencies in the plasma center, where $\omega_{\mathrm{cr}} = \pi / \tau_{\mathrm{cr}}$ assuming that half a turn is enough to detach particles from the reconnecting field lines [11] and ω_{vD} has been calculated with an orbit code. In the limit of $|q - 1| \ll 1$, $|\omega_{\mathrm{vD}}| / \omega_{\mathrm{cr}} \gtrsim 1$ is a criterion that fast ions may escape the reconnection (q being the safety factor). It is fulfilled in a broad region around $\xi = 0$, which is in qualitative agreement with the weak sawtooth redistribution measured in this area. Furthermore, it can be seen that $|\omega_{\mathrm{vD}}| / \omega_{\mathrm{cr}}$ increases strongly with the energy (logarithmic scale in fig. 7), which can explain why we measure lower relative changes around $\xi \approx 0$ with increasing energy.

4 Influence of RF heating on the beam ion distribution

The coupling of radio frequency (RF) waves to ions is an important physics aspect for future fusion devices. In ITER, 2nd harmonic ion cyclotron resonance heating of tritium is one of the foreseen ICRF schemes, along with He-3 minority heating. The 2nd harmonic heating has the benefit that it can accelerate the main ion species directly, however it is only efficient for ions with large Larmor radii (with respect to the RF wave length). At ASDEX Upgrade, the Larmor radii of D beam ions (i.e. from 60 keV NBI) are large enough for effective 2nd harmonic absorption.

We have analyzed discharge #30809, which has $B_{\mathrm{t}} = -2.4$ T and $I_{\mathrm{p}} = 1.0$ MA. The ICRF frequency is 36.5 MHz and the resonance layer is hence located at $R \approx 1.69$ m, i.e. very close to the magnetic axis. We have compared $t = 4.60$ s with 2.4 MW NBI + 1.8 MW ICRH and $t = 4.48$ s with 2.4 MW NBI only. FIDA data from four

views are available for this discharge. We have calculated tomographies from central lines of sight ($R \approx 1.75 - 1.78$ m), close to the ICRF resonance layer. The spectra of the $\Phi = 72°$ view are shown in fig. 9. It can be seen directly, that the FIDA spectrum is broader for $t = 4.60$ s, which indicates the presence of more energetic fast ions. The tomography is shown in fig. 10. It has to be noted, that in the presence of ICRF also fast H (minority) ions are expected to contribute to the Balmer-Alpha spectrum. The weight functions for hydrogen are almost identical with respect to the velocity (or E/m). Therefore, we have plotted the tomography as function of E/m and interpret it as the sum of fast D and fast H.

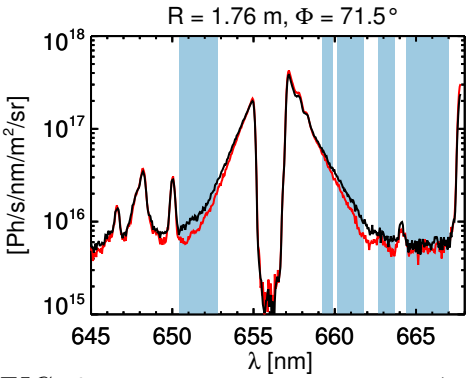

FIG. 9: FIDA spectrum for 4.48 s *(red) and* 4.60 s *(black). The blue shaded area is used for the tomography.*

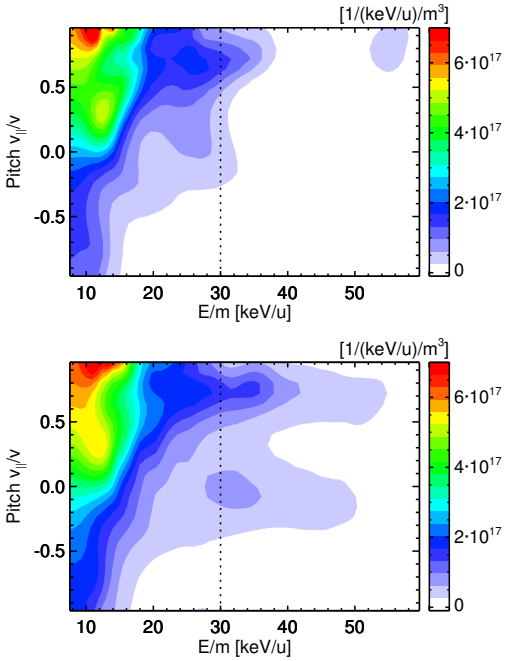

FIG. 10: FIDA tomography in the plasma center in the presence of 30 keV/u NBI and NBI+ICRF (down).

The NBI injection energy (30 keV/u) is indicated with a dotted line. At $t = 4.48$ s, the tomography yields mainly fast ions with energies below the injection energy, as expected. In the presence of ICRH ($t = 4.60$ s), two high energy tails are present. The stronger tail appears at pitches ≈ 0.7, and can be identified as beam ions, which are further accelerated. A second, weaker high energy tail is seen at pitches -0.3 to 0.0. It could originate from trapped ICRH-accelerated deuterium ions, which have the inner leg of their banana orbit at our measurement position with negative pitches. Hydrogen is expected to be accelerated up to much higher energies than accessible by the FIDA tomography (parallel temperatures of about 200-300 keV/u are expected). In the observed energy region, the H distribution function is expected to be rather uniform in velocity space, such that it can contribute to the overall absolute values, but cannot explain distinct features like the two observed energy tails. The tomography results can be directly compared to theoretical predictions, which will be presented in [13].

5 Summary and outlook

The recent upgrades of the FIDA diagnostic at ASDEX Upgrade allow a tomographic reconstruction of the fast-ion phase-space distribution function and hence phase-space resolved fast-ion studies. In the presence of sawtooth crashes, A 25% overall drop of fast-ion density is observed in the plasma center in line with a 19% increase at $\rho_{\mathrm{pol}} = 0.6$. For both positions, the strongest redistribution is seen for fast ions with pitch values close

to 1. The tomographic reconstruction allowed us to estimate the fast-ion redistribution quantitatively with resolution in energy and pitch. The basic trends are, however, already visible in the raw data, by comparing signals from different views. The pitch-angle dependence is in line with theoretical considerations [9, 10, 11], which explain it by the fact that ions with low $\left|v_\parallel/v\right|$ have large drift velocities (compared to their parallel velocity) and are thus more weakly bound to the (reconnecting) magnetic field lines.

The effect of ICRF heating on a beam ion distribution is clearly seen by high energetic tails in the tomography above the NBI injection energy. The pitch distribution of the energetic tails can be resolved, and two contributions at $\frac{v\|}{v} \approx 0.7$ (approx. same as NBI) and at $\frac{v\|}{v} \approx -0.15$ are found. A more detailed analysis will be presented in [13]: The radial dependence will be shown by tomographic reconstructions at six radial positions. This is in particular the first time, that a radial profile of 2D velocity space tomographies has been calculated. This is effectively equivalent with a three dimensional reconstruction of the phase-space (with the three dimensions being ion energy, pitch and radial position). Comprehensive comparisons with theoretical predictions from the TORIC modules in TRANSP and the TORIC-SSFPQL package will be presented. The analysis is completed with comparisons to other fast-ion diagnostics, in particular the active neutral particle analyzer and neutron rate measurements.

Acknowledgment

This work has been carried out within the framework of the EUROfusion Consortium and has received funding from the Euratom research and training programme 2014-2018 under grant agreement No 633053. The views and opinions expressed herein do not necessarily reflect those of the European Commission.

References

[1] Geiger B. et al., *Review of Scientific Instruments*, **84** (2013) .
[2] Weiland M. et al., *Plasma Physics and Controlled Fusion*, **58** (2016) 025012.
[3] Weiland M., PhD thesis, LMU München, 2016.
[4] Heidbrink W. et al., *Comm. Comp. Physics*, **10** (2011) 716.
[5] Geiger B., PhD thesis, LMU München, 2013.
[6] Anton M. et al., *Plasma Physics and Controlled Fusion*, **38** (1996) 1849.
[7] Geiger B. et al., *Plasma Physics and Controlled Fusion*, **57** (2015) 014018.
[8] Lovberg J. A. et al., *Physics of Fluids B: Plasma Physics*, **1** (1989) 874.
[9] Kolesnichenko Y. et al., *Nuclear Fusion*, **36** (1996) 159.
[10] Kolesnichenko Y. I. et al., *Physics of Plasmas*, **4** (1997) 2544.
[11] Jaulmes F. et al., *Nuclear Fusion*, **54** (2014) 104013.
[12] Geiger B. et al., *Nuclear Fusion*, **55** (2015) 083001.
[13] Weiland M. et al., Phase-space resolved measurement of 2nd harmonic ion cyclotron heating using FIDA tomography at the ASDEX Upgrade tokamak, *Nuclear Fusion*, (in preparation).